Waves generated by shear layer instabilities

By L. C. Morland[1], P. G. Saffman[1] and H. C. Yuen[2]

[1] *Department of Applied Mathematics, Caltech, Pasadena, California 91125, U.S.A.*
[2] *TRW Redondo Beach, California 90278, U.S.A.*

Stern & Adam and subsequent workers have considered the linear stability of two-dimensional, parallel, ideal fluid flow with shear in the presence of a free surface. In these studies a fluid current is modelled as a finite layer of constant vorticity above a semi-infinite stagnant region, corresponding to a piecewise-linear velocity profile. Here, an investigation of the stability of currents for several smooth velocity profiles is presented. With surface tension present it is found that the fluid surface velocity must still exceed the minimum wavespeed of stagnant fluid for instability to occur; a result highlighted by Caponi *et al.* for piecewise-linear profiles. Instability growth rates are found to be significantly smaller than those associated with a piecewise-linear profile. There are also qualitative differences in the stability characteristics; in particular, transition is associated with an exchange of stability for smooth profiles, but not for the piecewise-linear profile.

1. Introduction

In this paper, the instability mechanism for the generation of water waves discovered by Stern & Adam (1973), Voronovich *et al.* (1980), and discussed further by Caponi *et al.* (1991), is extended to the case of smooth velocity profiles. The cited authors considered the stability of a parallel, free surface flow in the particular case that the current in the water is represented by a layer of constant vorticity of depth Δ and surface velocity u_d, lying above a semi-infinite stagnant fluid region. In this model the role of a wind would be to produce a current in the water by viscous shearing. The effect of two-dimensional perturbations with dependence on the horizontal coordinate x, and time t, of the form $e^{i(kx-\sigma t)}$ was considered, where k is the wavenumber in the x-direction and σ is the angular frequency. The influence of the dynamics of the wind flow was neglected by taking the external pressure to be constant at the free surface. Stern & Adam and Caponi *et al.* applied continuity of velocity at the interface between the irrotational and rotational fluid layers and derived a cubic equation for the wavespeed $c = \sigma/k$. Voronovich & Lobanov applied continuity of pressure at the internal interface at which there was a vortex sheet; their analysis led to a quartic equation for the wavespeed c.

Solutions were found to exist for which c has a non-zero imaginary part corresponding to unstable modes. The unstable waves of interest are in the capillary-gravity régime with wavelengths of the order of centimetres; the viscous timescale is long enough that viscosity can be neglected in a first approximation to the instability problem (see equation (4.1)). (The influence of viscosity on the instability of the constant vorticity layer model was considered by Kawai (1977), who found that the effect was small.)

Caponi *et al.* showed that a necessary condition for unstable modes is that $u_d > c_m$,

Proc. R. Soc. Lond. A (1991) **433**, 441–450
Printed in Great Britain

where $c_m = (4gT)^{\frac{1}{4}}$ is the minimum capillary-gravity wavespeed for stagnant fluid, and that unstable modes then exist when the vorticity layer depth exceeds a critical value Δ_{crit}, which depends on u_d. Here, g is the acceleration due to gravity and T is the surface tension per unit density.

This model suggests that when a sufficiently strong wind picks up over a calm body of water there is initially no disturbance while vorticity diffuses into the fluid from the surface, and that waves spontaneously appear due to the instability of the fluid flow once the vorticity has penetrated into the fluid sufficiently and $\Delta > \Delta_{crit}$.

The mathematical tractability of the piecewise-linear velocity profile makes it attractive to work with. For instance, Milinazzo & Saffman (1990) computed steady finite amplitude waves of permanent form on a current with this profile by means of a Fourier series type expansion. However, the piecewise-linear profile has a discontinuity in the first derivative at the internal interface and there is a common belief that not only quantitatively but qualitatively incorrect results can be predicted by piecewise-linear profiles. In this paper we present the results of a numerical investigation of three smooth profiles and compare the results with the piecewise-linear profile.

The mathematical formulation of the stability of inviscid flow in a semi-infinite domain with a free surface differs from the stability of parallel flows of boundary layer type only in the free surface boundary condition. The latter problem has received considerable attention (for a recent review, see Drazin & Reid (1981)). Squire's transformation, which states that to every three-dimensional disturbance there corresponds a two-dimensional disturbance (see Drazin & Reid, p. 129), still holds with a rescaling of the physical parameters. As a consequence only the two-dimensional stability problem need be solved. We also find that the corollary for rigid walls that for every unstable three-dimensional disturbance there exists a more unstable two-dimensional disturbance can also be derived for the free surface problem; see equation (4.2).

Two other important results in the theory of parallel flow instability are Rayleigh's inflection point theorem, which states that a necessary condition for inviscid instability is that the velocity profile has an inflection point; and Howard's semicircle theorem, which states that in the complex c-plane unstable modes must lie in the semicircle of diameter $(U_{max} - U_{min})$ with centre equidistant between U_{min} and U_{max} on the real axis. U_{max} and U_{min} are respectively the maximum and minimum velocities of the current $U(y)$, where y is a coordinate measured vertically upwards. The free surface problem has been examined by Yih (1972), who derives some results analogous to those known for the boundary layer problem. In particular he shows that Howard's semicircle theorem extends to the free surface flow. He also derives some sufficient conditions for stability; however, they are not applicable to the velocity profiles being considered here as we are interested in profiles without points of inflection that would be set up by a wind blowing with approximately constant speed and direction. For such a profile U_y and U_{yy} are both positive throughout the fluid. In his abstract Yih states that unstable modes are not possible unless there exists a mode for which $c \in (U_{min}, U_{max})$; the unstable modes, if they exist, are then contiguous to this neutral mode. Such a neutral mode can only be part of the discrete spectrum of Rayleigh's equation (equation (2.4a)) if the velocity profile has an inflection point. Hence in his abstract Yih implies that Rayleigh's theorem also holds for the free surface flow. However, this result is not proved in the main body of the paper and our results show it not to be the case.

2. Mathematical formulation

Cartesian coordinates are defined with the x-axis lying along the undisturbed surface. The position of the free surface is given by $y = \eta(x, t)$, where t is time. The fluid velocity $\boldsymbol{u} = (u, v)$ and pressure p of an incompressible, inviscid fluid under the influence of gravity satisfy the Euler equations and the equation of continuity,

$$\boldsymbol{u}_t + \boldsymbol{u}\cdot\nabla\boldsymbol{u} = -\nabla p + \boldsymbol{g}, \tag{2.1a}$$

$$\nabla\cdot\boldsymbol{u} = \boldsymbol{0}, \tag{2.1b}$$

where the fluid density has been put equal to unity, $\boldsymbol{g} = -g\boldsymbol{j}$ and $\boldsymbol{j}$ is a unit vector in the y-direction. The free surface boundary conditions are continuity of pressure and the requirement that the free surface is a material surface of the fluid, i.e.

$$p = -T\eta_{xx}/(1+\eta_x^2)^{\frac{3}{2}} \quad \text{on} \quad y = \eta, \tag{2.2a}$$

and

$$\eta_t + \boldsymbol{u}\cdot\nabla\eta - v = 0 \quad \text{on} \quad y = \eta. \tag{2.2b}$$

At large depths the fluid velocity is required to decay to zero,

$$\boldsymbol{u} \to 0 \quad \text{as} \quad y \to -\infty. \tag{2.2c}$$

The undisturbed state is a steady parallel flow solution of the boundary value problem given by (2.1) and (2.2) with $\boldsymbol{u} = (U(y), 0)$, pressure given by the hydrostatic law $p = -gy$, and the fluid surface planar, $\eta = 0$. With small, time dependent two-dimensional perturbations the velocity and pressure are $\boldsymbol{u} = (U+u', v')$, $p = -gy + p'$ and the free surface is $y = \eta'$, where $|p'|$, $|u'|$, $|v'|$ and $|\eta'| \ll 1$. Neglecting products of small quantities in equations (2.1) and (2.2) gives the standard equations

$$u'_t + Uu'_x + U_y v' = -p'_x, \tag{2.3a}$$

$$v'_t + Uv'_x = -p'_y, \tag{2.3b}$$

$$u'_x + v'_y = 0 \tag{2.3c}$$

in the fluid, and

$$\eta'_t + U\eta'_x - v' = 0 \quad \text{on} \quad y = 0, \tag{2.3d}$$

$$p' = g\eta' - T\eta'_{xx} \quad \text{on} \quad y = 0, \tag{2.3e}$$

and

$$(u', v') \to 0 \quad \text{as} \quad y \to -\infty. \tag{2.3f}$$

We seek normal mode solutions of the form $u' = \mathrm{i}\phi_y(y)\,\mathrm{e}^{\mathrm{i}(kx-\sigma t)}/k$, $v' = \phi(y)\,\mathrm{e}^{\mathrm{i}(kx-\sigma t)}$ and $\eta' = a\,\mathrm{e}^{\mathrm{i}(kx-\sigma t)}$, where k is the streamwise wave number and σ is the angular frequency, possibly complex. To obtain physical quantities the real parts of the above expressions are to be taken; ϕ is in general complex valued. Eliminating the pressure between (2.3a) and (2.3b) gives Rayleigh's equation,

$$\phi_{yy} - (k^2 + U_{yy}/(U-c))\,\phi = 0, \tag{2.4a}$$

where $c = \sigma/k$ is the wavespeed. Eliminating η' between (2.3d) and (2.3e) gives the free surface boundary condition,

$$(U-c)^2\phi_y - (U_y(U-c) + g + Tk^2)\,\phi = 0 \quad \text{on} \quad y = 0 \tag{2.4b}$$

and the boundary condition at infinity, (2.3f), requires that

$$\phi \to 0 \quad \text{as} \quad y \to -\infty. \tag{2.4c}$$

Equations (2.4) form an eigenvalue problem for c.

If c is real and lies in the range of U, i.e. $c \in (U_{\min}, U_{\max})$, then (2.4$a$) has a regular singular point at any point y_s where $U(y_s) = c$. Such values of c with an appropriate jump condition applied to ϕ at the singularity make up the continuous spectrum. To

solve the general initial value problem for small disturbances requires consideration of the continuous spectrum. However, our primary concern is with instability and hence with wavespeeds with non-zero imaginary part. These are contained in the discrete spectrum and have proper eigenfunctions and hence can be found via the normal mode analysis.

In the case of the piecewise-linear profile, U_{yy} is proportional to a delta function with singularity at $y = -\Delta$. As a consequence ϕ has distinct analytic representations in the rotational and irrotational regions. Stern & Adam and Caponi *et al.* applied continuity of velocity at the interface and hence, as is well known, continuity of pressure follows since the fluid density is uniform.

For the purposes of comparing the stability characteristics of different profiles it is necessary to have criteria for profiles to be similar. Since the piecewise-linear profile is determined by specifying the fluid surface velocity and the vorticity layer thickness, two profiles are considered to be comparable if both of these quantities are equal. The natural definition for the fluid surface velocity is $u_d = U(0)$. The definition of Δ is less obvious and we take the simplest possibility which is twice the depth of the vorticity centroid,

$$\Delta = \frac{2}{u_d}\int_{-\infty}^{0} U(y)\,\mathrm{d}y. \tag{2.5}$$

Three families of smooth profiles are considered in this paper; the exponential profile, the error function profile, and the integrated error function profile, given respectively by

$$U(y) = u_d\,\mathrm{e}^{2y/\Delta}, \quad -\infty < y < 0, \tag{2.6a}$$

$$U(y) = u_d\,\mathrm{erfc}\,(-2y/\sqrt{\pi}\Delta), \quad -\infty < y < 0, \tag{2.6b}$$

$$U(y) = u_d\left(\exp\left(-\frac{y^2\pi}{4\Delta^2}\right)+\frac{\pi y}{2\Delta}\,\mathrm{erfc}\left(-\frac{y\sqrt{\pi}}{2\Delta}\right)\right), \quad -\infty < y < 0. \tag{2.6c}$$

An attractive feature of the exponential profile is that an analytic solution can be found with $c = 0$ which determines the neutral stability curve.

The error function profile (2.6*b*) is appropriate for the case of a wind which instantaneously sets the fluid surface in motion with constant speed u_d. For example, a laminar wind with velocity $(1+(\nu_\mathrm{w}/\nu_\mathrm{a})^{\frac{1}{2}}(\rho_\mathrm{w}/\rho_\mathrm{a}))\,u_d$ at a large height above the water surface, where ν and ρ are kinematic viscosity and density and subscripts w and a indicate water and air respectively, sets up the profile (2.6*b*) with Δ growing like

$$\Delta = 4\sqrt{(\nu_\mathrm{w} t/\pi)}. \tag{2.7}$$

The integrated error function profile (2.6*c*), which results in a time-dependent u_d, is appropriate for the case when the current is set up by a constant stress τ on the surface. For a laminar flow, $u_d = 2\Delta\tau/\mu_\mathrm{w}\pi$, where Δ is now given by

$$\Delta = \sqrt{(\pi\nu_\mathrm{w} t)}. \tag{2.8}$$

This profile lies almost midway between the exponential and error function curves.

By scaling lengths with the wavelength λ, and velocities with the capillary-gravity wavespeed $c_0 = \sqrt{(g\lambda/2\pi + 2\pi T/\lambda)}$, the parameter dependence is reduced to u_d/c_0 and Δ/λ. With this scaling of variables indicated by a 'hat' (^), equations (2.4) become

$$\hat{\phi}'' - (4\pi^2 + \hat{U}''/(\hat{U}-\hat{c}))\,\hat{\phi} = 0 \tag{2.9a}$$

$$(\hat{U}-\hat{c})^2\hat{\phi}' - (\hat{U}'(\hat{U}-\hat{c}) + 2\pi)\,\hat{\phi} = 0 \quad \text{on} \quad y = 0, \tag{2.9b}$$

$$\hat{\phi} \to 0 \quad \text{as} \quad y \to -\infty, \tag{2.9c}$$

where the prime now indicates differentiation with respect to $\hat{y}$. Note that this equation has no explicit dependence upon the two parameters, which enter through the profile $\hat{U}(\hat{y})$. In all cases, $\hat{U}(0)$ is u_d/c_0 and $\hat{U}'(0)$ is proportional to $(u_d/c_0)(\lambda/\Delta)$.

It follows that the eigenvalue problem (2.9) has solutions of the form

$$\hat{c} = c/c_0 = \hat{C}(\lambda/\Delta, c_0/u_d), \tag{2.10}$$

where $\hat{C}$ depends only on the profile and the parameters. In particular, for each profile the marginal stability curve $\mathrm{Im}\,(c) = 0$ is a fixed curve in the $\lambda/\Delta - c_0/u_d$ plane.

To determine c as a function of λ for given u_d and Δ, say, we note that c_0 and λ are of course not independent but related by the linear dispersion relation which we write as

$$\left(\frac{c_0}{u_d}\right)^2 = \frac{1}{2}\left(\frac{c_\mathrm{m}}{u_d}\right)^2\left[\left(\frac{\lambda}{\Delta}\right)\left(\frac{\Delta}{\lambda_\mathrm{m}}\right)+\left(\frac{\lambda_\mathrm{m}}{\Delta}\right)\left(\frac{\Delta}{\lambda}\right)\right]. \tag{2.11}$$

Here, $\lambda_m = 2\pi(T/g)^{\frac{1}{2}}$ is the wavelength of the slowest capillary-gravity wave. Thus the stability properties are determined by the values of $\hat{C}$ on the locus (2.11) in the $\lambda/\Delta - c_0/u_d$ plane. The dimensional growth rate σ_i is given by

$$\sigma_i = k\,\mathrm{Im}\,(c) = 2\pi\frac{u_d}{\Delta}\frac{c_0}{u_d}\frac{\Delta}{\lambda}\mathrm{Im}\,(\hat{C}). \tag{2.12}$$

For the case of zero surface tension, the equivalent locus to (2.11) is

$$\left(\frac{c_0}{u_d}\right)^2 = \frac{\Delta g}{2\pi u_d^2}\frac{\lambda}{\Delta}. \tag{2.13}$$

Numerical solution of equations (2.9) was performed by fixing the parameters and solving iteratively for $\hat{c}$ and $\hat{\phi}$. (Actually, we did not solve (2.9) but another set of equations obtained by scaling speeds and lengths with c_m and λ_m, which proved to be more convenient in practice.) Equations (2.9*a*) and (2.9*b*) were replaced by second-order accurate finite difference approximations; an asymptotic condition being used for (2.9*c*). The approximations to (2.9*a*) and (2.9*c*) plus a normalization condition, $\hat{\phi}'(0) = 1$, led to a tri-diagonal system for the discrete approximation to $\hat{\phi}$. This system was solved in each step of an application of the secant method to equation (2.9*b*); each refinement to $\hat{c}$ adjusts the approximation to $\hat{\phi}$ through (2.9*a*). This numerical procedure was found to converge rapidly to the solution except when the true value of $\hat{c}$ had a small imaginary part in which case a very accurate initial estimate for $\hat{c}$ and a fine grid for the finite difference approximations were required.

For the exponential profile the $\hat{C} = 0$ neutral curve can be determined analytically in the $\lambda/\Delta - c_0/u_d$ plane and is

$$\lambda/\Delta = \tfrac{1}{2}\pi(1-(c_0/u_d)^4)/(c_0/u_d)^2. \tag{2.14}$$

3. Results

Numerical results for the smooth profiles are now presented and compared with results for the piecewise-linear profile. Figure 1 is a sketch of the loci in the complex c-plane of the wavespeeds of the two discrete modes associated with a smooth profile as the wavelength varies, when there is instability for the case of capillary-gravity waves, i.e. $u_d > c_\mathrm{m}$ and $\Delta > \Delta_\mathrm{crit}$. Also included in the diagram is the unstable section of the equivalent loci for a piecewise-linear profile.

The horizontal and vertical axes are the real and imaginary parts of c respectively

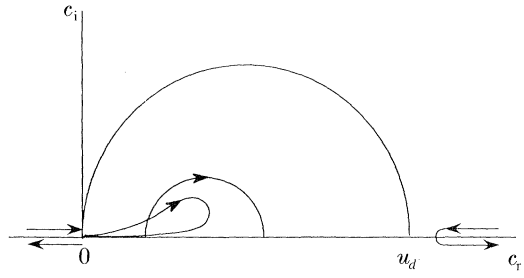

Figure 1. A sketch of the wavespeeds in the complex c-plane as the wavelength varies for a smooth profile when there is instability, shown by the 'tongue' emanating from $c = 0$. Also included are the unstable wavespeeds for a piecewise-linear profile, shown by the part ellipse. The large semicircle is the Howard semicircle.

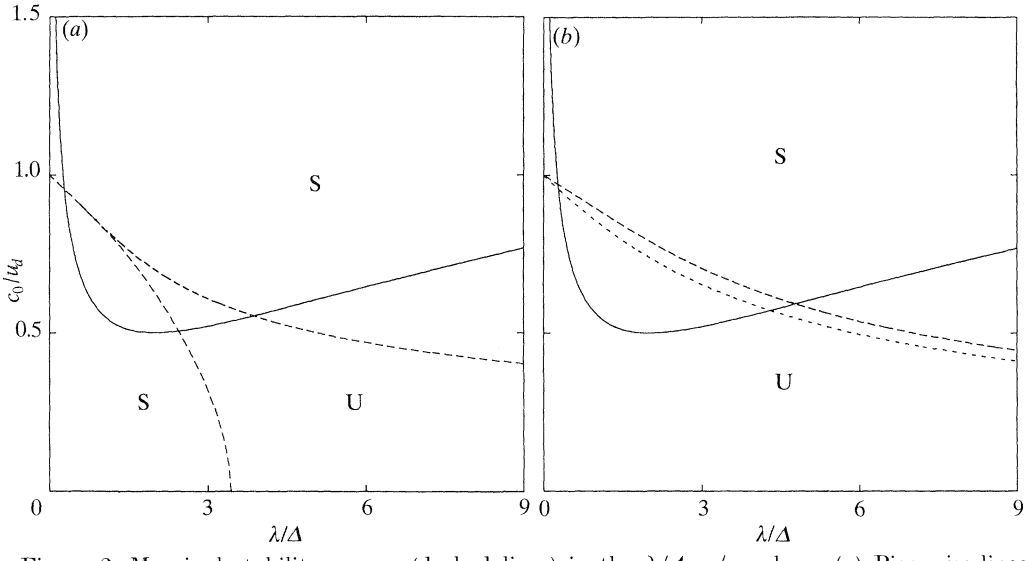

Figure 2. Marginal stability curves (dashed lines) in the λ/Δ–c_0/u_d plane. (a) Piecewise-linear profile. (b) Smooth profiles: – – –, exponential profile; ————, error function profile. The curve for the integrated error function lies between the two others. The solid line is the locus (2.11) drawn for $u_d/c_m = 2$, $\Delta/\lambda_m = 0.5$. The stable and unstable regions are indicated by S and U respectively.

and the arrows indicate the direction of decreasing λ. The semicircle passing through $c = 0$ is the boundary of the region in which wavespeeds with non-zero imaginary part must lie, as required by the extension of Howard's semicircle theorem. When a mode is unstable, only the wavespeed with positive imaginary part is shown. The loci of neutrally stable modes, which lie on the real axis, are shown parallel to and displaced from the axis for clarity.

The two modes shown in figure 1 correspond to the well-known capillary-gravity waves that occur on stagnant fluid. As $\lambda \to \infty$ the influence of the current diminishes and hence the wavespeeds tend to those of long waves on stagnant fluid, $|c| \sim (g\lambda/2\pi)^{\frac{1}{2}}$. Figure 1 shows that as λ decreases from infinity the wavespeed of the mode with positive velocity decreases, attains a minimum and then increases again. For small wavelengths the mode is convected with the surface velocity and so $c \sim u_d + (2\pi T/\lambda)^{\frac{1}{2}}$. The minimum velocity is found to be greater than u_d and hence by the semicircle theorem this mode is always stable.

The wavespeed of the second mode is large and negative at both large and small wavelengths. At some intermediate wavelength the phase speed has a maximum; if the physical parameters u_d and Δ are such that this value is positive then the semicircle has been penetrated and instability is possible. Our results show that for a smooth profile, instability occurs as the real part of c becomes positive; the wavespeed locus departs tangentially from the real axis at $c = 0$. The locus ultimately returns to $c = 0$ through smaller values of the imaginary part of c, tracing out the 'tongue' shown in figure 1. Because the convective entrainment of the wave speed is less than u_d, the speed of the second mode can only be positive if $u_d > c_m$.

The transition to instability for the smooth profiles is an exchange of stability, i.e. $c = 0$ when $\mathrm{Im}\,(c) = 0$. This is not the case for the piecewise-linear profile, which in addition to the capillary gravity-like modes has a discrete mode associated with the vorticity layer. The phase speed of the vorticity mode is bounded by zero and the fluid surface velocity, taking the value u_d at infinite wavelength and tending to zero as the wavelength tends to zero. Instability occurs as a result of collisions on the $\mathrm{Re}\,(c)$-axis between the slow capillary-gravity like mode and the vorticity mode; consequentially the former mode does not become unstable immediately upon entering the semicircle and a piecewise-linear profile has narrower bands of unstable wavelengths than a smooth profile. Here 'collision' is used to mean that two distinct modes have the same wavespeed at the same wavelength. The part ellipse in figure 1 sketches the instability locus in the complex c-plane for the piecewise-linear profile. The details of the collisions on the real axis leading to the instability locus have been omitted.

Voronovich *et al.* noted that these collisions produce instability because they are between modes with energy of opposite sign. It is of interest to interpret the production of instability by a smooth profile in terms of energy; however, we are not aware of a satisfactory definition for the energy of an infinitesimal rotational disturbance to a flow of non-uniform vorticity.

When surface tension is absent, the phase velocities of the modes associated with the smooth profiles are monotonic functions of wavelength and tend to u_d as the wavelength tends to zero. In the case of the unstable mode, the wavespeed tends to u_d through complex values.

Figure 2*a* and *b* show the marginal stability curves ($\mathrm{Im}\,(c) = 0$) and neutral curves ($c = 0$) in the $\lambda/\Delta - c_0/u_d$ plane for the piecewise-linear and smooth profiles respectively. These are shown by dashed lines. It should be emphasized that these lines are functions only of the profile. The solid lines in figure 2 are the loci given by equation (2.11). These depend on the values of u_d/c_m and Δ/λ_m. Those shown are for $u_d/c_m = 2$ and $\Delta/\lambda_m = 0.5$. For fixed values of u_d and Δ, instability occurs when the value of λ is such that the solid line lies inside the instability regions, which for the smooth profiles is below the dashed line. The minimum of the solid line occurs when $c_0 = c_m$ and $\lambda = \lambda_m$. It follows again that instability can only occur if $u_d > c_m$. As Δ decreases, the solid line moves to the right. It follows that for each value of u_d, there is a minimum value of Δ which we have called Δ_{crit}, such that instability can only occur when $\Delta > \Delta_{crit}$. When $\Delta = \Delta_{crit}$, the solid line is tangent to the dashed line.

The marginal stability curve for the piecewise-linear profile, figure 2*a*, differs qualitatively from the neutral curves, figure 2*b*, for the smooth profiles in that it consists of two branches; the instability region is the wedge bounded by the two. The smooth profiles have neutral stability curves consisting of a single branch and the region of instability lies below the curve. Thus the piecewise-linear profile stabilizes

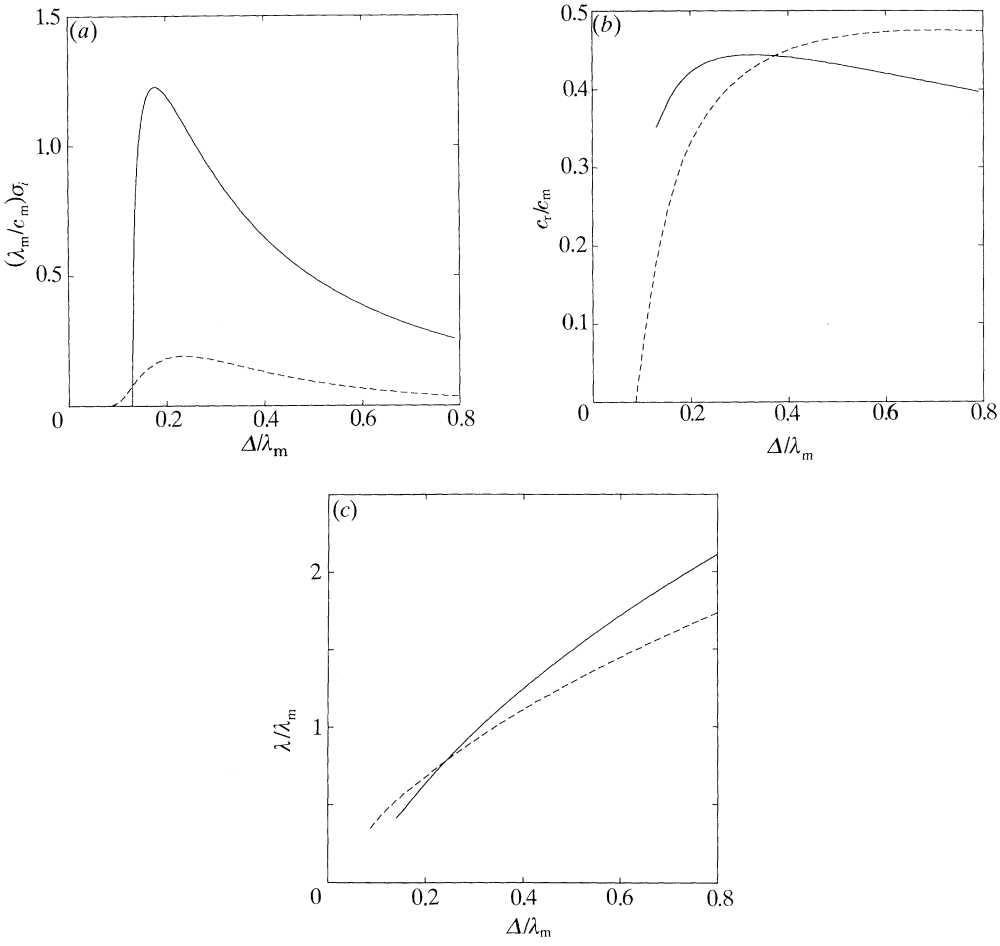

Figure 3. Properties of most unstable waves as functions of vorticity layer thickness for $u_d/c_m = 2$. (*a*) Growth rate; (*b*) phase speed; (*c*) wavelength. ——, Piecewise-linear profile; – – –, error function profile.

when Δ becomes large, but the growth rates of the smooth profile instabilities are found to be so small when Δ is large that this difference is more apparent than real. Figure 2 also shows that the upper branch of the marginal stability curve of the piecewise-linear profile lies close to the marginal stability curves of the smooth profiles and hence that both profile types give similar values of Δ_{crit}. Indeed, the piecewise-linear profile reproduces quite well the dependence of the geometry of the instability region on the various parameters.

With zero surface tension the dashed curves in figure 2*a* and *b* remains unaltered. However, the solid line locus is now given by equation (2.13). It can be seen that for any non-zero u_d and Δ there are always unstable modes for small enough λ.

In figure 3*a* the maximum growth rates of the piecewise-linear and error function profiles are compared over a range of Δ for $u_d/c_m = 2$. The figure demonstrates the much larger growth rates of the piecewise-linear profile when compared with a smooth profile. The exponential profile has smaller growth rates than the error function profile and the growth rates of the integrated error function lie between the

Table 1. *The most unstable wave at a range of values of* u_d/c_m
((*a*) Piecewise-linear profile; (*b*) error function profile; (*c*) integrated error function profile; (*d*) exponential profile.)

	u_d/c_m	Δ/λ_m	λ/λ_m	c_r/c_m	$\lambda_m \sigma_i/c_m$
(*a*)	1.75	0.250	0.653	0.323	0.602
	2.0	0.175	0.541	0.404	1.226
	2.25	0.135	0.481	0.483	2.069
	2.5	0.105	0.408	0.551	3.136
(*b*)	1.75	0.299	0.823	0.263	0.051
	2.0	0.234	0.764	0.369	0.191
	2.25	0.187	0.707	0.467	0.475
	2.5	0.150	0.649	0.553	0.936
(*c*)	1.75	0.313	0.843	0.236	0.025
	2.0	0.245	0.785	0.336	0.109
	2.25	0.197	0.732	0.432	0.294
	2.5	0.161	0.681	0.520	0.617
(*d*)	1.75	0.372	0.870	0.235	0.008
	2.0	0.291	0.817	0.333	0.043
	2.25	0.235	0.767	0.430	0.137
	2.5	0.194	0.722	0.522	0.319

two. Also shown are the corresponding wavelengths and phase speeds in figure 3*b* and *c*. In contrast with the growth rates the phase speeds and wavelengths are similar for the two profiles. Table 1*a–d* give details of the wave of maximum growth rate at different values of u_d for the four profiles. The tables show the sensitivity of growth rate to profile type and the relative insensitivity of vorticity layer thickness, wavelength and phase speed.

4. Comments

This paper has been concerned with instabilities arising in free surface flow when the current has a smooth velocity profile, and a comparison has been made with the piecewise-linear profile. Our numerical results using three distinct smooth profiles show that the profiles have qualitatively the same behaviour with good quantitative agreement, except that the growth rates for the piecewise-linear profile are an order of magnitude larger.

The analysis has been based on the assumption that the velocity profiles are quasi-steady. That is, the time for viscosity or turbulence to modify the profiles is assumed large compared with the time for the disturbance to grow. The condition for this to hold is

$$\sigma_i \gg \nu/\Delta^2, \quad \text{i.e.} \quad \nu \ll \tfrac{1}{20} c_m \Delta, \tag{4.1}$$

according to the data shown in figure 3*a* and table 1.

Squire's transformation enables us to compare the growth rates of three-dimensional disturbances. For a three-dimensional disturbance proportional to $e^{i(\alpha x+\beta z)}$ under the influence of gravity g and surface tension per unit density T, the standard approach (see, for example, Drazin & Reid 1981) shows that for a given profile the three-dimensional and two-dimensional growth rates are related by,

$$\sigma_{3D}\left(\alpha\lambda_m, \beta\lambda_m, \frac{\Delta}{\lambda_m}, \frac{u_d}{c_m}\right) = \frac{\alpha}{\bar{\alpha}}\sigma_{2D}\left(\bar{\alpha}\bar{\lambda}_m, \frac{\Delta}{\bar{\lambda}_m}, \frac{u_d}{\bar{c}_m}\right), \tag{4.2}$$

where $\bar{\alpha} = (\alpha^2+\beta^2)^{\frac{1}{2}}$, and $\bar{c}_{\mathrm{m}}$ and $\bar{\lambda}_{\mathrm{m}}$ are respectively the minimum wavespeed and corresponding wavelength associated with scaled gravity and surface tension given by $\bar{g} = (\bar{\alpha}/\alpha)^2 g$ and $\bar{T} = (\bar{\alpha}/\alpha)^2 T$. To compare the growth rates of the three-dimensional disturbance with a two-dimensional disturbance under the influence of the same gravity and surface tension, (4.2) is rewritten as

$$\sigma_{3D}\left(\alpha\lambda_{\mathrm{m}}, \beta\lambda_{\mathrm{m}}, \frac{\Delta}{\lambda_{\mathrm{m}}}, \frac{u_d}{c_{\mathrm{m}}}\right) = \frac{\alpha}{\bar{\alpha}}\sigma_{2D}\left(\bar{\alpha}\lambda_{\mathrm{m}}, \frac{\Delta}{\lambda_{\mathrm{m}}}, \frac{\alpha u_d}{\bar{\alpha} c_{\mathrm{m}}}\right), \tag{4.3}$$

by noting that λ_{m} is unaffected by the scaling of g and T, and c_{m} is multiplied by $\bar{\alpha}/\alpha$. Hence a non-zero β is equivalent to a reduced surface velocity and consequently the maximum growth rate is less than that for $\beta = 0$. There is therefore a directional selection mechanism in this instability.

These results are for profiles without inflection points. A gusty wind can be expected to produce inflexion points in the undisturbed profiles of velocity, which will presumably produce instabilities with much larger growth rates. This is a problem for further study.

We thank Dr S. Cowley for many helpful discussions and in particular his advice concerning the numerics. Partial financial support by the Office of Naval Research (Grant N000-14-89-J-1164) is gratefully acknowledged.

References

Caponi, E. A., Yuen, H. C., Milinazzo, F. A. & Saffman, P. G. 1991 Water wave instability induced by a drift layer. *J. Fluid Mech.* (In the press.)

Drazin, P. G. & Reid, W. H. 1981 *Hydrodynamic stability*. Cambridge University Press.

Kawai, S. 1977 On the generation of wind waves relating to the shear flow in water. A preliminary study. *Sci. Rep. Tohoku Univ.* ser. 5, Geophys. **24**, 1–17.

Milinazzo, F. A. & Saffman, P. G. 1990 Effect of a surface shear layer on gravity and gravity-capillary waves of permanent form. *J. Fluid Mech.* **216**, 93–112.

Stern, M. E. & Adam, Y. A. 1973 Capillary waves generated by a shear current in water. *Mém. Soc. r. Sci. Liége*, 6$^{\mathrm{e}}$ série, **6**, 179–185.

Voronovich, A. G., Lobanov, E. D. & Rybak, S. A. 1980 On the stability of gravitational-capillary waves in the presence of a vertically nonuniform current. *Izv. atm. Ocean Phys.* **16**, 220–222.

Yih, C. S. 1972 Surface waves in flowing water. *J. Fluid Mech.* **51**, 209–220.

Received 26 November 1990; accepted 10 January 1991